International Journal of Mechanical and Thermal Engineering

E-ISSN: 2707-8051
P-ISSN: 2707-8043
IJMTE 2024; 5(1): 41-55
Received: 11-12-2024
Accepted: 16-01-2024

Abdulrazzaq M Saleh Aljumaily
Department of Mechanical Engineering, College of Engineering Alsharqat University of Tikrit, Iraq

Alaa AM Hayes Al-Jubouri
Department of Mechanical Engineering, College of Engineering Alsharqat University of Tikrit, Iraq

Nour FH Al-Jubouri
Department of Mechanical Engineering, College of Engineering Alsharqat University of Tikrit, Iraq

Corresponding Author:
Abdulrazzaq M Saleh Aljumaily
Department of Mechanical Engineering, College of Engineering Alsharqat University of Tikrit, Iraq

Improving the Thermal Storage System (LHTES): A theoretical and experimental study

Abdulrazzaq M Saleh Aljumaily, Alaa AM Hayes Al-Jubouri and Nour FH Al-Jubouri

DOI: https://doi.org/10.22271/27078043.2024.v5.i1a.56

Abstract
The research aims to enhance the thermal efficiency of a thermal storage system by altering the geometric shapes of the inner tube through theoretical and experimental studies. Six inner tube forms were selected: Pentagonal, hexagonal, square, rectangular, circular, and elliptical, all with the same outside surface area. Paraffin wax, a phase transition substance, is deposited in the shell, while water, a Heat Transfer Fluid (HTF), flows through the inner tube at a rate of two liters per minute. A 3D simulation was performed using the Computational Fluid Dynamics (CFD) software ANSYS Fluent 2020 R2 for all chosen geometric shapes. The findings suggest that the circular tube outperformed the other forms examined in terms of absorbing heat from the PCM through the HTF.

Keywords: Heat exchanger, solidification, shell and tube, phase change material, and energy storage.

1. Introduction
Energy serves as a crucial catalyst for global development, with the everyday growth in energy consumption worldwide. Renewable energy is being more widely used, recognized as a pivotal energy resource and a resilient solution against environmental changes. Renewable energy, sourced from natural elements like wind, hydropower, and solar, stands out as the most typical and sustainable sources. Despite fossil fuels currently contributing to almost 80 percent of the global energy supply, renewable energy emerges as the world's fastest-growing energy source. Addressing the challenges in energy utilization and generation necessitates the production of Thermal Energy Storage Systems (TESS). Within systems for storing thermal energy, PCM-based latent heat storage systems (LHSS) are especially well-suited for a variety of possibilities. Latent Heat Thermal Energy Storage (LHTES) systems have been the subject of numerous experimental and numerical studies aimed at improving and optimizing their thermal efficiency.

Du *et al.* [1] conducted a comprehensive examination of PCM applications across various temperature ranges, encompassing power generation, heating, and cooling. Azain *et al.* [2] and Alva [3] delved into the utilization of paraffin wax PCM in heat exchangers. Paraffin wax emerged as a suitable medium for storing thermal energy, as observed by Senthil *et al.* [4] and Jesumathy *et al.* [5] in a horizontal heat exchanger. Rathod *et al.* [6] carried out a comparable investigation in a heat exchanger that is vertical, Erythritol was PCM of choice for Wang *et al.* [7] in their vertical heat exchanger-based latent heat thermal storage unit. Jalal and Salih [8] offered a numerical investigation of paraffin wax's impact on double-glazed windows' behavior.

Tangsiriratana *et al.* [9] introduced an innovative approach, In a solar panel-integrated system with PCM (EPCM), Sugar cane wax's Al2O3 compound serves as the foundational material, while Gum Arabic is employed as the polymer shell. In a cylindrical encapsulation inside a solar air heater, In his work, Abed [10] utilized PCM-sand for combined latent and sensible heat storage materials, while opting for just sand for sensible heat storage materials. Meanwhile, Abbas*et al.*'s [11] experimental study incorporated PCM capsules as insulating materials and identified the optimal placement of these capsules within a wall.

According to a detailed numerical analysis of the influence of PCM location in LHTESUs by Mahdi *et al.* [12], discharging in state a happened noticeably faster than in state B, with an overall discharging time that was 43.4% shorter.

According to their research, tubular heat exchangers can be equipped with multi-layer PCM, Sadeghi *et al.* [13] recommended adding more PCM layers to improve latent heat absorption.

Nevertheless, as noted within the studied range by Liu *et al.* [14], Alshara *et al.* [15], and Elmeriah *et al.* [16], the solidification process of stearic acid exhibits negligible sensitivity to the Reynolds number for the cooling water. Avci *et al.* [17] and Agarwal *et al.* [18] have shown that the melting process advances radially upward due to buoyant forces, with the top part experiencing a quicker than the bottom part's melting time.

Seddegh *et al.* [19] examined natural convection using both computational and experimental techniques in a vertical tube/shell latent thermal energy storage system LTESS. Natural convection regulates the initial discharge process before switching to conduction, according to the research. It's interesting to note that this behavior differs from the melting process, where natural convection predominates and is linked to buoyancy forces, as explained by Jesumathy *et al.* [5]. Furthermore, as Hosseini *et al.* [20] noted, from the pipe to the shell, the border of the molten material advances, and as HTF temperature rises, the melting time gets shorter. Moreover, the inner tube's use of eccentric geometric forms produces an amplified impact.

Certain factors and discharge time were shown to be correlated by Yazici *et al.* [21]. A longer melting period of PCM was observed when the number of tubes in the shell was reduced, and reduce the average Nusselt number, as observed by Esapour *et al.* [22] as reported by Kousha *et al.* [23]. He *et al.* [24] Demonstrated that changing the diameter of the inner aluminum tube resulted in a corresponding decrease in the temperature of PCM. Shen *et al.* [25] found that HTF tube position inside the multi-tube storage unit had a major impact on the PCM's thermal performance.

In their experimental and computational investigation, Kibria *et al.* [26] examined the vertical LHTES, taking into account several scenarios in which HTF is fed from both the bottom and upper sides through the stages of melting and solidification. Maximum efficiency within the vertical LHTES framework was found while feeding during solidification from the lower side and during melting from the opposite side. Furthermore, the length of the solidification/melting process was significantly impacted by the pipe's radius. According to Korawan *et al.* [27], the shell/nozzle design had the longest period of intense convection, followed by the shell/tube configuration and the shell/reduce arrangement. Moreover, numerical simulations were carried out by Seddegh *et al.* [28] in order to validate against published experimental results.

The effects of adjusting the inclination angle of a heat exchanger containing phase change materials—like stearic acid by Mehta *et al.* [30] and paraffin wax by Kousha *et al.* [29] have been studied. The results show that during the first half of the operation, PCM's average temperature drops from 0° to 90° as the inclination angle rises. Siyabi *et al.* [31] suggest doing more study to examine how the inclination angle affects PCM storage systems, paying particular attention to techniques like fins that improve heat conductivity.

Soheil *et al.* [32] numerically examined how various inner tube shapes (diamond-like, square, elliptical, and rectangular) influence the performance of a cylindrical PCM storage system. According to the data, there are no appreciable variations in the charging times for 75% of the PCM across all configurations. Moreover, Da and Meyer *et al.* [33] found that using a semicircular thermal exchanger instead of the inner tube of a traditional tube-in-tube heat exchanger significantly increased the heat transfer efficiency. On the other hand, the heat exchanger that Al-Jabair and Althaea [34] looked at had an inner spiral tube that had different spiralling degrees.

In addition to testing and comparing different finned tube heat exchangers, Longeon *et al.* [35] will use graphite foam to increase PCM thermal conductivity. By employing twisted tape as a tabulator and (CuO/distilled water and Al_2O_3) as the working fluid, Fouad and Aljabair [36] improved the thermal performance of exchangers.

Esapour *et al.* [37] examined the incorporation of PCM with porous metal foam while examining a horizontal multi-tube heat storage system. According to their research, adding metallic foam and using more inner tubes significantly accelerates the rates of solidification and melting. Moreover, Ghalambaz and Zhang *et al.* [38] explored the effect of fusion temperature, external cooling power, and Biot number on a heatsink made of metal foam and paraffin wax in terms of its thermal performance. Their investigation revealed that adjusting these external parameters led to an increase in heatsink efficiency.

Albaldawi *et al.* [39] state that reducing the external cooling power (Biot number) improves efficiency and that the Thermal Energy Storage Unit's necessary charging time is shortened by using Copper Lessing Rings coated in paraffin wax. Copper nanoparticles and porous steel/nickel alloys serve as media to enhance the two-dimensional melting of ice/water within an inclined elliptical annulus. Especially in oblate topology the usage of Nanostructured Encapsulated Phase Change Material (NEPCM) has shown beneficial when conductive heat transmission predominate Jourabian *et al.* [40].

In hexagon/tube settings Begum *et al.*, [42] and shell/tube configurations Wang *et al.*, [41], the melting and solidification processes are significantly influenced by mass flow rate and intake HTF temperature. It was shown that the mass flow rate of HTF has an opposing impact on stored energy and significantly affects the times of solidification and melting. An analytical tool for analyzing the kinetics of heat transfer between HTF and PCM is the numerical approach known as "Iterating alternately between thermal resistance and temperature in a different manner", which was developed by Kibria *et al.* [26].

The purpose of the study was to evaluate two different LHTES unit configurations. A horizontal heat exchanger with one design had a PCM-filled shell and a tube holding the HTF, while the other design had the PCM-filled tube and the HTF-containing shell. According to Mahdi *et al.* [12], the results showed a notable 50% decrease in PCM melting time for the second arrangement, which was ascribed to convection's strong impact.

A reduced mass flow rate of HTF was suggested by Akgun *et al.* [43] as a tactic to reduce energy usage. Furthermore, they observed that when the temperature of the HTF's input rose, the melting time shortened, this agrees with the conclusions reached by Jian-you *et al.* [44] and Hosseini *et al.* [45].

To comprehend the convective currents regulating the buoyant force amid PCM melting within a heat exchanger positioned horizontally, Hosseini *et al.* [46] carried out a

combined computational and experimental investigation. The results showed that at higher HTF temperatures, the melt front moved from the pipe to the shell and the melting time decreased. The study demonstrated that convection had a major role in solidification and that conduction affected melting.

Two different configurations of (LHTES) units were used in a numerical study by Mahdi *et al.* [11]. A horizontal heat exchanger with a PCM-filled shell and an HTF-filled pipe was part of the original setup. The second arrangement, on the other hand, was the opposite. As a result of convection's increased influence, the second configuration's PCM melting time was found to be 50% shorter.

The research aims to enhance the thermal storage system's performance by altering the geometric shapes of the inner tube. Six different tube forms were selected for theoretical and practical study: Circular, hexagonal, pentagonal, square, rectangular, and elliptical tubes. The water flow rate used was 2 litters per minute.

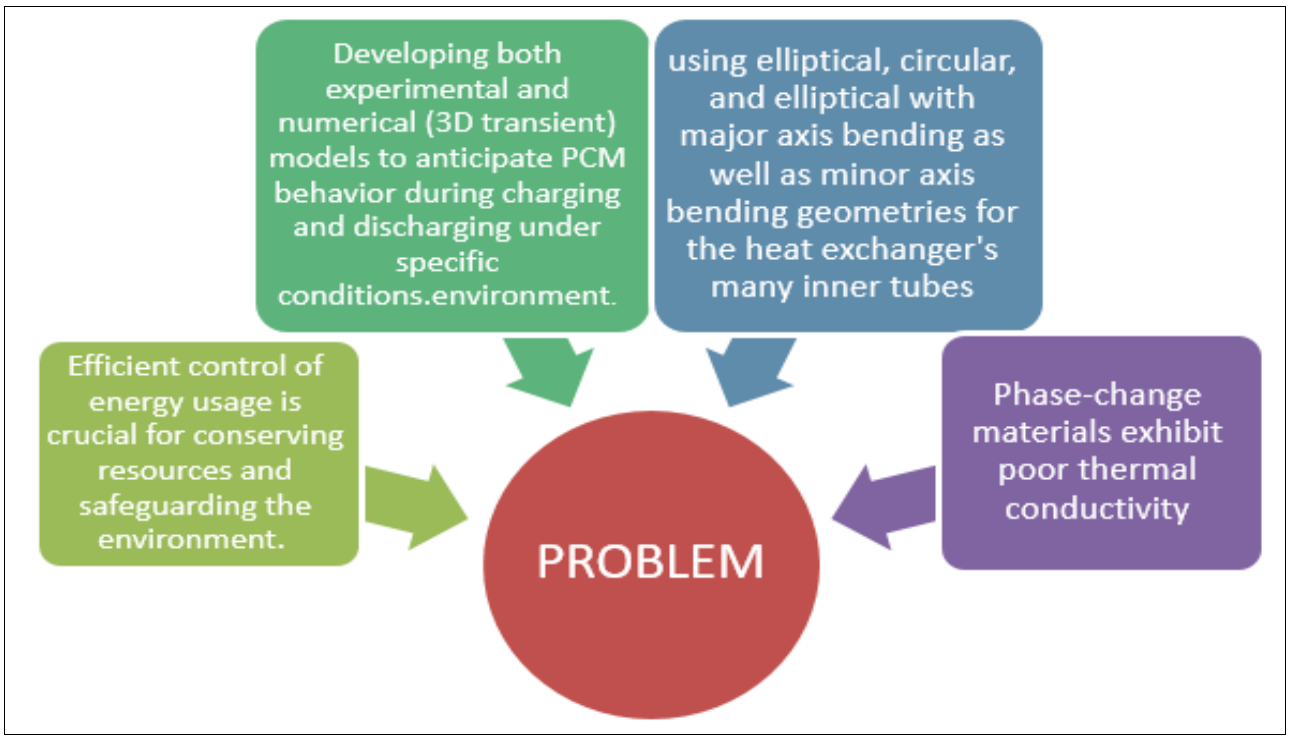

Fig 1: Problem Synopsis

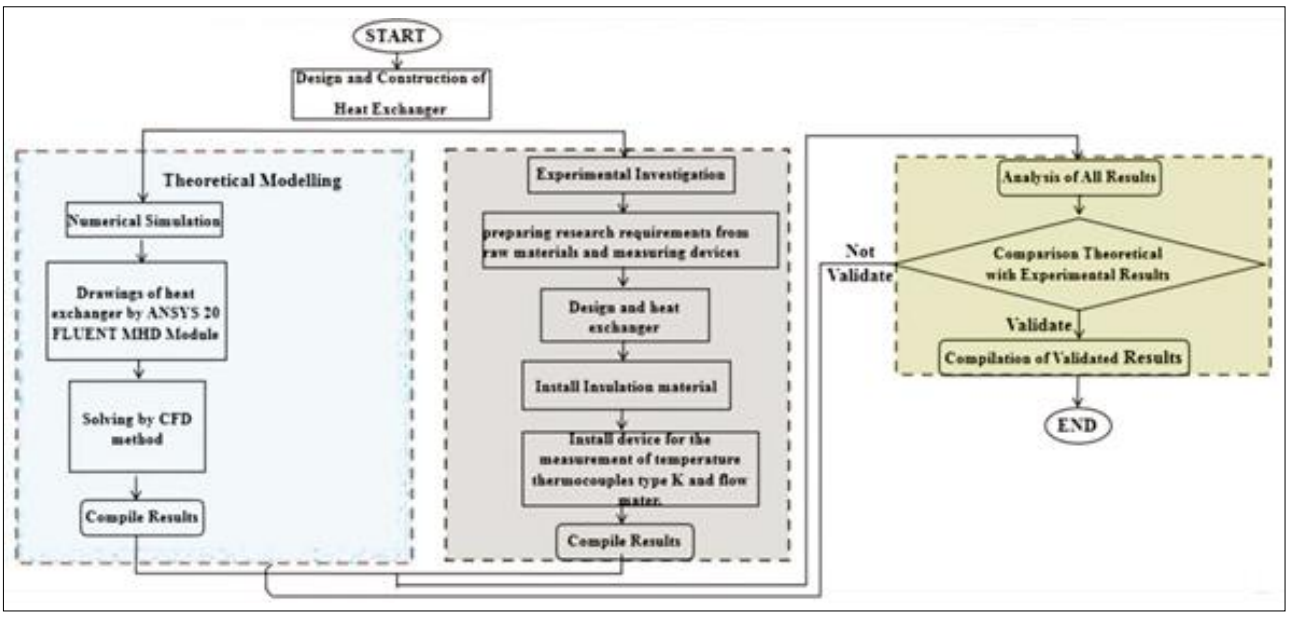

Fig 2: Methods of Research

2. Experimental program

2.1 Apparatus and Procedures

Figure 3 shows the device used in the experiments. While Figure (4) shows the layout of the entire experimental device. An inner tube and a shell make up the heat storage system. The external shell has a diameter of 154.08 mm and a length of 1.28 meters. It is 7.11 mm thick and composed of carbon steel. The two holes on top and bottom make it easier to fill and drain wax. There are four sections to the shell (A, B, C) that are separated by 0.32, 0.64, and 0.96

meters. To measure the wax temperature throughout its axis, nine thermocouples were positioned at various angles (0°, 45°, and 90°) in each zone. The HTF water was directed using three internal concentric tube configurations. The inner tube is circular and manufactured of carbon steel. It has a diameter of 52.48 mm, a length of 2000 mm, and a thickness of 3.91 mm. Four annular heaters, each with a diameter of 169 mm and a combined power output of 4200 W, were employed on the exterior of the shell to melt the paraffin wax. Three layers of insulation were applied to the test portion to minimize heat loss to the surrounding environment. The initial layer comprises a ceramic fibber blanket with a thickness of 0.0025 m and a thermal conductivity of at least 0.153 W/m•K. The second layer consists of glass wool composed of sintered glass fiber with a thickness of 0.001m and a thermal conductivity ranging from 0.026 to 0.042W/m. The third layer was constructed from tin with a thickness of 0.0005 meters, and its thermal conductivity coefficient typically fell within the range of 50 to 66 W/m K. To encase the crust externally. The heat transfer fluid is provided from a 67.5-liter galvanized water tank. The 0.5 HP water pump can extract liquid water from the main tank at a rate of 30 liters per minute. Two thermocouples were positioned at the water intake and exit. Paraffin wax sourced from the Al-Dora refinery in Iraq was utilized, and its thermal and physical characteristics were quantified, as detailed in Table 1.

Fig 3: System of experimentation

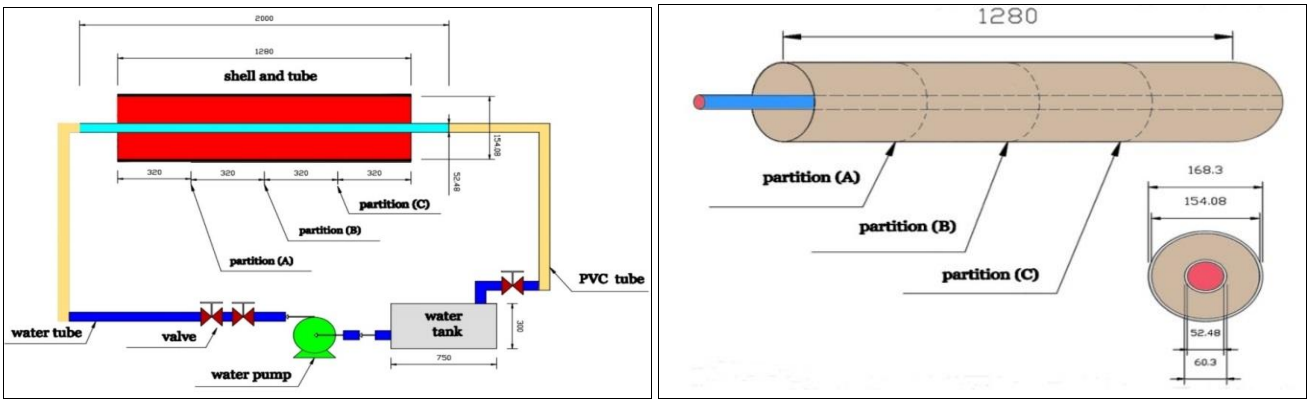

Fig 4: The experimental setup's schematic design.

Table 1: Properties of used materials thermo-physical

Materials Properties	Paraffin Wax (PCM)	Water	Copper	Insulation
Thermal expansion coefficient [1/K]	0.000307	-	-	-
Thermal conductivity in solid state [W / m K]	0.259	-	387.6	0.043
Specific heat in liquid state [J/kg K]	2460	4182	-	-
Density in solid state [kg/m3]	894.56	-	8978	-
Dynamic viscosity [kg/m s]	0.01405	0.001003	-	-
Specific heat in solid state [J/kg K]	1659	-	381	-
Melting temperature [K]	334	-	-	-
Thermal conductivity in liquid state [W / m K]	0.158	0.6	-	-
Liquidous temperature [K]	339	-	-	-
Latent heat of fusion [J / kg]	235512.5	-	-	-
Solidus temperature [K]	318.5	-	-	-

In TESS, the melting or solidification processes rely on the temperatures of the water at the input and outflow, which act as the immediate energy transfer's heat transfer fluid. The following is an expression for the equations [46].

$$q_{ch} = m\ C_P\ (T_{f,\text{in}} — T_{f,out}) \quad (1)$$

$$q_{dis} = m\ C_P\ (T_{f,\text{out}} — T_{f,in}) \quad (2)$$

$$Q_{ch\&dis} = \sum q_{dis\&ch}\Delta t \quad (3)$$

Where $T_{f,in}$ $T_{f,out}$ denotes the temperatures of the intake and exit water, CP stands for mass flow rate, and HT for specific heat.

The transient state process can be used to formulate the energy cumulative melting/solidification equation as follows:

$$Q_{H.E,} = M_{H.,\,E}\,(T_{end} — T_{ini}) \quad (4)$$

$$Q_{H.E,,} = M_{H.E}\,C_{p,\,H.E}\,(T_{ini} — T_{end}) \quad (5)$$

In this case, T_{ini} and Tend indicate PCM beginning and ending temperatures during the operation, while $C_{p,\,H.E.,}$ and $M_{H.E.}$ Stand for the specific heat, mass, and mass of the heat exchanger section when empty. The subsequent equation represents the total exchangeable energy utilizing PCM.

The following is the expression for LHTES theoretical efficiency:

$$\eta_{THEO} = \frac{Q_{PCM,dis\ \&ch}}{Q_{max,dis\ \&ch}}$$

The following formula may be used to calculate the maximum theoretical energy that is transferred throughout the melting and solidification processes using PCM.

$$Q_{max,\,dis} = [C_P\,(T_{ini} — T_{liquidus}) + C_P\,(L * F)\,(T_{liquidus}\ T_{solidus})] \quad (7)$$

$$Q_{max,\,ch} = [(T_{ini} — T_{solidus}) + C_{P\ pcm}\,(L * F)\,(T_{end} — T_{liquidus})] \quad (8)$$

The PCM C_P PCM specific heat and mass, M_{pcm} solidus and liquidus temperatures, $T_{liquidus}$ $T_{solidus}$, the liquid fraction (F), and the latent heat of fusion (L) are all represented by the symbols.

2.2 Uncertainty Analysis

To ensure robust practical outcomes, it is crucial to assess result reliability. Numerous researchers engage in uncertainty analysis, which entails evaluating uncertainties linked to various variables to precisely determine the overall experimental error This entails linking a collection of independent variables, such (Y1, Y2, Y3……., Y_n\) etc. (Holman 2011) [47], with a variable, like T, obtained via a practical test.

$$T = T\,(Y_1, Y_2, Y_3 \ldots\ldots Y_n) \quad (10)$$

The correlation between the proportions of certain differences in the variables is shown by the equation that is given.

$$\partial N = \frac{\partial T}{\partial Y1}\partial Y1 + \frac{\partial T}{\partial Y2}\partial Y2 + \frac{\partial T}{\partial Y3}\partial Y3 + \cdots + \frac{\partial T}{\partial Yn}\partial Yn \quad (11)$$

The uncertainty of the findings (RT) is stated as follows:

$$RT = \left[\left(\frac{\partial T}{\partial Y1}R1\right)^2 + \left(\frac{\partial T}{\partial Y2}R2\right)^2 + \left(\frac{\partial T}{\partial Y3}R3\right)^2 + \cdots + \left(\frac{\partial T}{\partial Yn}Rn\right)^2\right]^{\frac{1}{2}} \quad (12)$$

Equation 12 divided by Equation 10 yields the following:

$$\frac{RT}{T} = \left[\left(\frac{\partial T}{\partial Y1}\frac{R1}{T}\right)^2 + \left(\frac{\partial T}{\partial Y2}\frac{R2}{T}\right)^2 + \left(\frac{\partial T}{\partial Y3}\frac{R3}{T}\right)^2 + \cdots + \left(\frac{\partial T}{\partial Yn}\frac{Rn}{T}\right)^2\right]^{\frac{1}{2}} \quad (13)$$

The temperature and mass flow rate measurements' inaccuracies, caused by the equipment used for measuring flow rate and temperature, are 4% and 0.75%, respectively. Several other factors contribute to the potential inaccuracies in the heat transfer rate equation

$$Q = F\,(\Delta T, \dot{m}) \quad (14)$$

$$\frac{\partial Q}{\partial \dot{m}} = C_p\,\Delta T \quad (15)$$

$$\frac{\partial Q}{\partial \Delta T} = C_p\,\dot{m} \quad (16)$$

$$Q_{PCM,\,dis\,\&,h} = Q_{\,ch\&dis} — Q_{H.E,\,dis\&ch} \quad (6)$$

The uncertainty in heat transmission (RQ) can be expressed as follows:

$$\frac{R_Q}{Q} = \left[\left(\frac{\partial Q}{\partial \dot{m}}\ \frac{R_{\dot{m}}}{Q}\right)^2 + \left(\frac{\partial Q}{\partial \Delta T}\ \frac{R_{\Delta T}}{Q}\right)^2\right]^{\frac{1}{2}} \quad (17)$$

Where

$$R_m = error_{\,\dot{m}}\,\dot{m} \quad (18)$$

$$R_{\Delta T} = error_{\Delta T}\Delta T \quad (19)$$

Replace the values of all terms in Equation A-8.

$$\frac{R_Q}{Q} = 6\%$$

2.3 Numerical simulation

Using a numerical simulation, the effect of altering internal geometries on the heat transfer process from PCM to HTF during discharging is examined. The simulations were conducted using the ANSYS-Fluent 2020 R2 program, and PCM discharge was described using the enthalpy technique By using this method, the disruptions and energy balance issues associated with solid/liquid contact are avoided. It's interesting to note that it tracks the solid-liquid boundary indirectly by using the liquid fraction (F). The analysis is predicated on the following assumptions:

- Prerequisites for unstable states in three dimensions (3-D).
- Newtonian fluid properties, laminar flow, and incompressible behavior for HTF.
- The uniform, isotropic characteristics of the phase change material.
- A constant temperature of 299 K for the water (HTF) intake.
- Not enough consideration is given to vessel dissipation
- No heat escapes to the outside because the outside of the shell is fully insulated. Heat transfer only occurs between the phase change material (PCM) and the heat transfer fluid (HTF).

The energy equation contains the formula for both temperature and total volumetric enthalpy:

$$\frac{\partial \rho H}{\partial t} + \nabla.(\rho V H) = \nabla.(K\nabla T) + C \quad (20)$$

In the above equation, velocity is represented by V, the source term is C, thermal conductivity is denoted by k, and total volumetric enthalpy (H) is the sum of the sensible and latent heats.

$$H = H + FL \tag{21}$$

$$H = H_{REF} + \int_{TREF}^{T} C_P dT \tag{22}$$

Where F is the liquid percentage, which ranges between 0 and 1 in the mushy zone, and C_p represents the specific heat, while HREF signifies the enthalpy at the reference temperature TREF, which is 299 K.

$$F = \begin{cases} 0 & T < Ts \\ \frac{T-Ts}{T_L-Ts} & T_L \leq T \leq Ts \\ 1 & T > T_L \end{cases} \tag{23}$$

Equation 2 and 4 are substituted into Equation 1 to create the following energy equation:

$$\frac{\partial \rho H}{\partial t} + \nabla.(\rho VZ) = \nabla.(K\nabla T) - \frac{\partial \rho FL}{\partial t} - \nabla.(\rho VFL) + C \tag{24}$$

When the momentum equation may be written as follows, and L is the latent heat of fusion:

$$\frac{\partial \rho}{\partial t} + \nabla.(\rho vv) = -\nabla P + \nabla.(\mu \nabla V) + \rho g + \frac{(1-F)^2}{F^3+\varepsilon} VA_{mush} \tag{25}$$

A modest number, ε = 0.001, prevents division by zero, While considering the constant in the soft region, $Amush = 10^5$, Functions as a velocity-damping factor during the discharge of PCM.

The Bossiness approximation approach can be utilized to tackle the problem of a tiny density difference. This entails setting reference values for temperature (T_0), density (ρ_0), and thermal expansion coefficient (β), assuming that the fluid density stays constant, and eliminating a body force factor from the momentum equation.

The momentum equation may thus be written as follows:

$$\frac{\partial \rho_0 v}{\partial t} + \nabla.(\rho_0 vv) = -\nabla P + \nabla.(\mu \nabla v) + (\rho - \rho_0)g + \frac{(1-F)^2}{F^3+\varepsilon} VA_{mush} \tag{26}$$

$$(\rho - \rho_0)\, g = \beta\, \rho_0\, (T - T_0) \tag{27}$$

One way to compute the continuity is to use:

$$\frac{\partial \rho}{\partial t} + \nabla.(\rho v) = 0 \tag{28}$$

2.4 Numerical Setup

Well-defined problem geometry is necessary in order to solve the analyzed case numerically using Fluent CFD. Six different geometric shapes make up the inner tube construction: Hexagonal, pentagonal, square, rectangular, elliptical, and circular tubes 3.1.1 Case Study's Geometry.

2.5 Mesh Independence Test

In order to reduce the error and increase the accuracy of the numerical simulation results, a grid independence test was performed. To avoid differences in calculations, five alternative numbers were chosen for the sample grid elements, and the overall fraction was used to determine the appropriate number. According to the results, the mesh element sizes were determined for hexagon (elements: 223913), pentagon (elements: 116017), square (elements: 83640), rectangle (elements: 46000): 48843), oval (elements: 146422), circular (elements: 165236), (Fig 4).

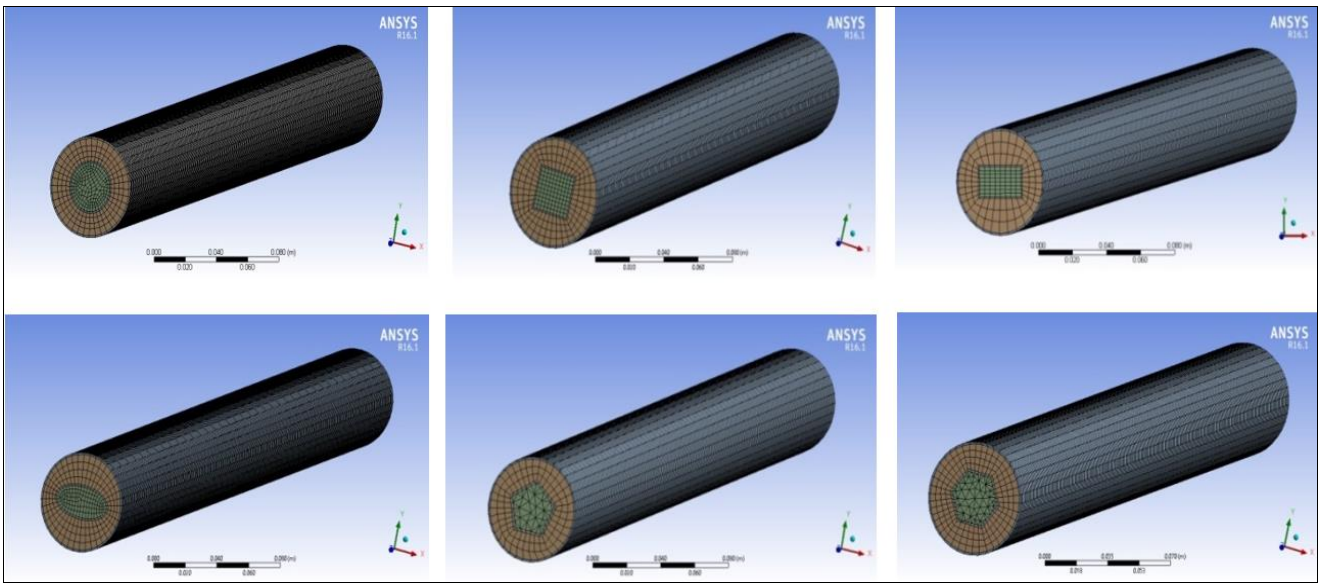

Fig 5: Generating meshes involves configurations such as shell/circular tube, shell/square tube, shell/rectangular tube, shell/elliptical tube, shell/pentagonal tube and shell/hexagonal tube

2.6 Setup Solver

A time period must be established in order to solve the equations, and the time step size that is selected determines this period. Based on real-world outcomes, choosing the right number of time steps is crucial. A time step size of 1 s produced a desirable result. To guarantee solution

convergence at every step, the maximum iteration value was set to 1 for every time step. After testing different time step sizes, it was determined that 1000 time steps was the optimal temperature for PCM initialization, which was set at 349.8776 K. The pressure-velocity coupling was controlled by the SIMPLE algorithm, which used a second-order upwind estimation for the momentum and energy equations, a second order for the pressure energy equation, and an implicit first-order method for the transient formulation. The liquid fraction, density, pressure, body forces, momentum update, and energy under-relaxation factors were set at 1, 0.3, 1, 0.9, 0.7, and 1, in that order.

2.7 Boundary Conditions

To simulate the solidification process and solve the equations, as well as analyse the temperature distribution, different geometries were taken into account, and the selected state parameters are shown in Figure 5.

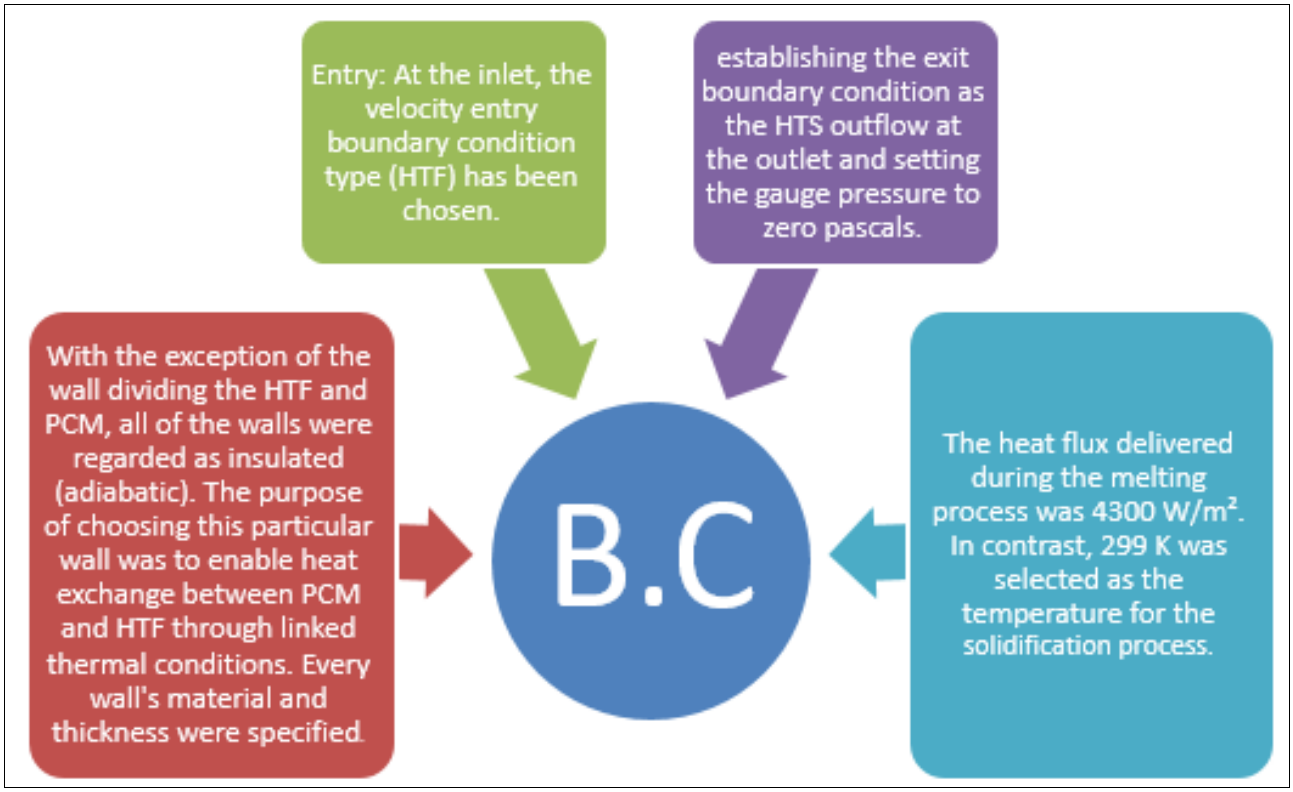

Fig 6: Demonstrate how boundary conditions are selected by numerical simulation

3. Results and Discussion

At 298 K, the degassing procedure begins with cold water maintained at a constant temperature, and recordings are made after the PCM has melted at 345 K. For each simulation test, this cycle is repeated while changing the internal geometries (circular tube, square tube, rectangular tube, elliptical tube, pentagonal tube, hexagonal tube). In each case, the numerical solution produces acceptable values. The heat flux produced during the melting process was 4300 W/m². In contrast, 298 K was chosen as the temperature for the solidification process. Except for the wall separating the HTF and PCM, all walls were considered insulated (thermal material). The purpose of choosing this particular wall was to enable heat exchange between the PCM and HTF through associated thermal conditions. The material and thickness of each wall were specified. The gauge pressure is set to zero Pa and the exit boundary condition is determined as flow of heat transfer fluid at the outlet. Input: At the inlet, the Entry Speed Limit Condition (HTF) type is selected.

3.1 Influence of Heat Transfer on Discharging

It is necessary to distinguish the mutual relationship between the two basic methods of heat transfer, namely heat transfer by conduction and natural convection during the discharge process. The following figures (2-D and 3-D) show the liquid fraction and temperature for different volumetric flow rates of HTF (2 L/min) in six geometries. The effect of changing the inner tube geometry on the discharge process behavior of the LHTESS unit can be explained as follows. Figures (6 and 7) show the liquid ratio and temperature in the case of the circular tube/inner shell at 2 litres/min. The figures show that fast convection currents initially control the PCM discharge process due to the buoyant force. This accelerates heat exchange and PCM discharge starting from the inner tube towards the outer tube. After that, the conductive heat transfer becomes stronger and thus takes longer to finish discharging. PCM discharge begins at an angle of (0^0) on the horizontal axis, then an angle of (45^0) on the diagonal axis, followed by (90^0) on the vertical axis. Due to the low conductivity of paraffin wax and the slow growth of the solid, a layer of paraffin wax is formed near the inner tube. Moreover, one of the reasons why the temperature in section (A) is lower than in sections (B) and (C) is that there is significant heat transfer between the HTF and PCM in the first section of the test heat exchanger. For the case (square tube, rectangular tube, oval tube, pentagonal tube, hexagonal tube)/shell at (2 L/min), the temperature curves are shown in Fig 6 and 7. These numbers show behavior similar to what was described previously. Although the temperature distribution and liquid mass lines over radial distance indicate that the discharge time is shorter compared to the case of a circular

inner tube. In summary, the greatest theoretical and experimental heat transfer was in the outer/inner circular tube Moreover, the maximum theoretical and experimental cumulative energy value was for the outer tube/circular tube. Furthermore, the maximum thermal and experimental efficiency was for the outer/inner circular tube.

3.2 Combining the current study's experimental and numerical results

The findings show that, in terms of temperature distribution, the numerical calculations and experimental testing agree satisfactorily, as shown in Fig. 8.

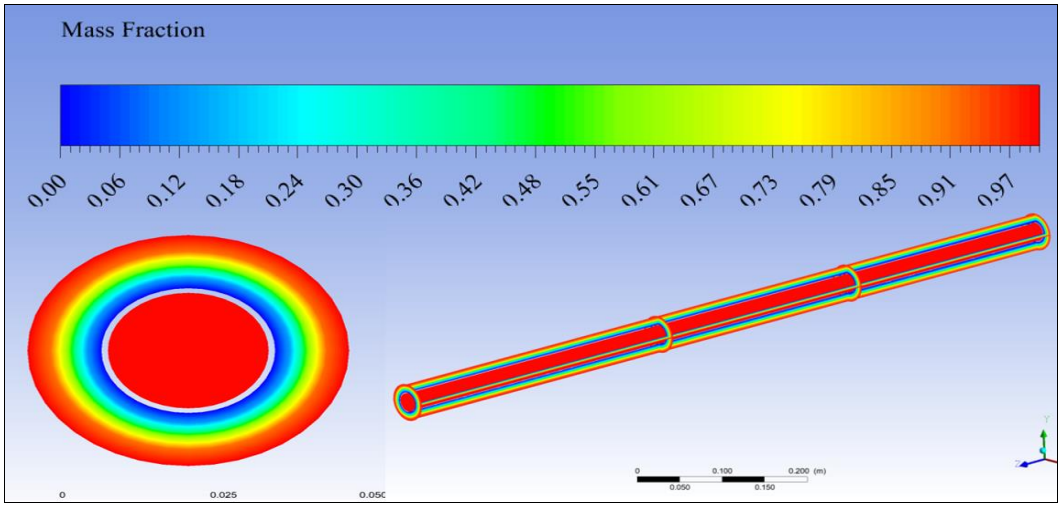

A. The mass fraction of the circular tube

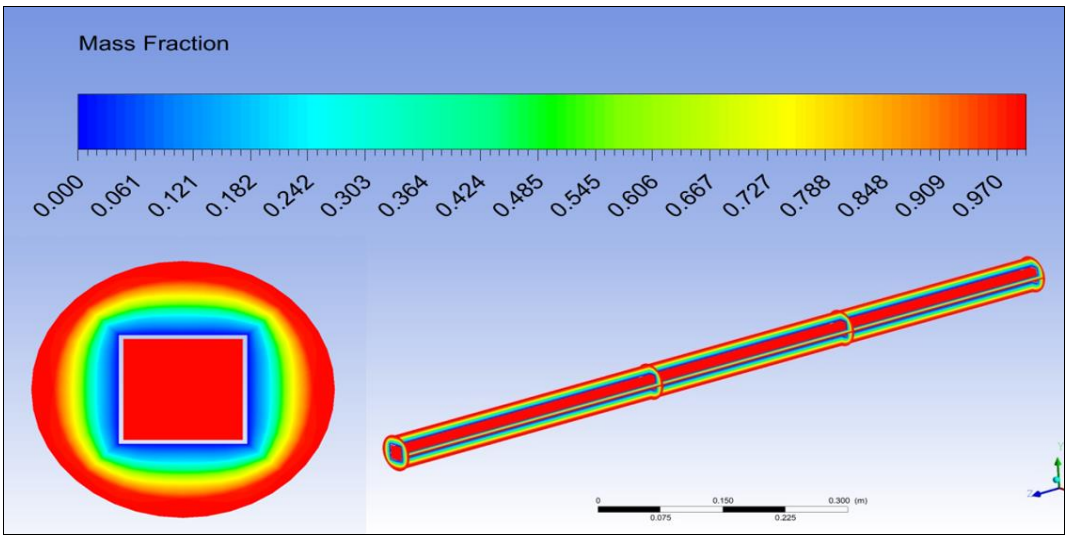

B. The mass fraction of the Square tube

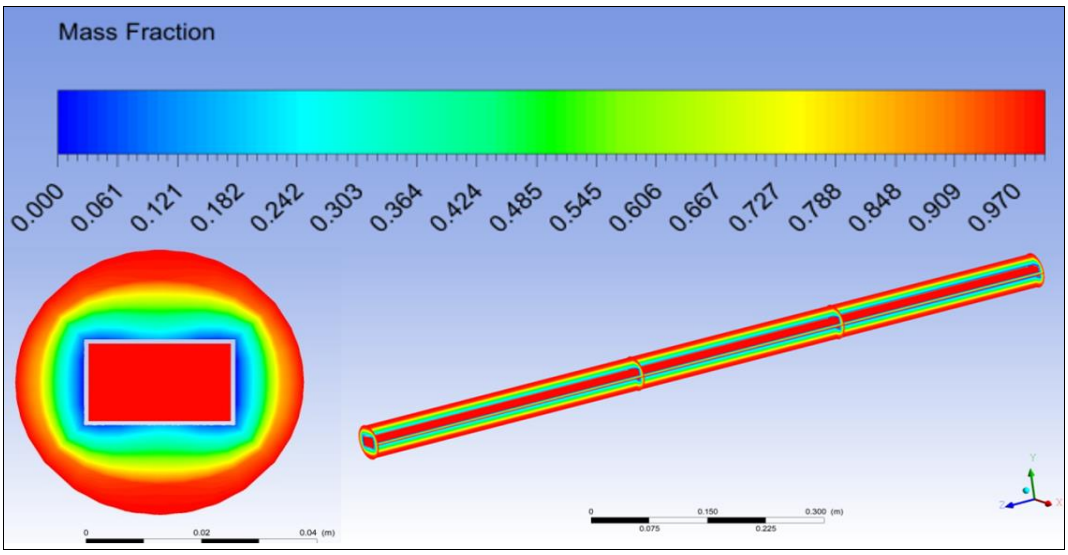

C. The mass fraction of the rectangular tube

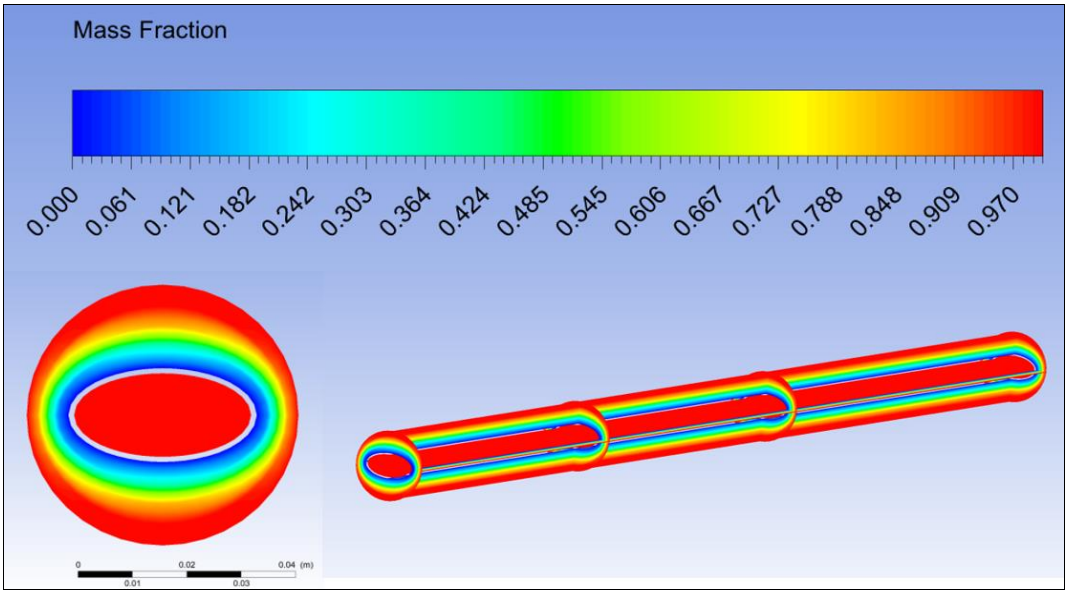

D. The mass fraction of the elliptical tube

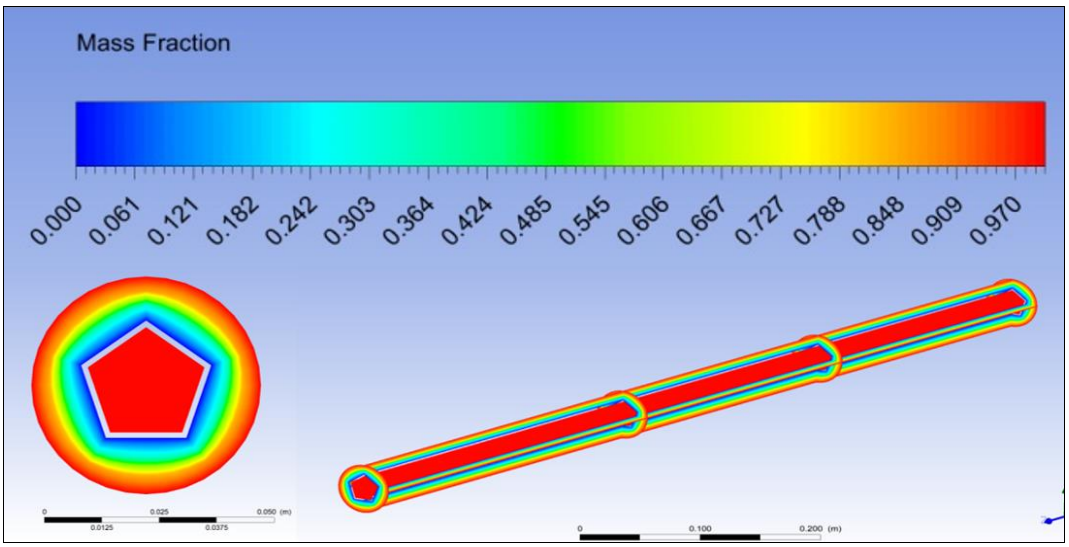

E. The mass fraction of the pentagonal tube

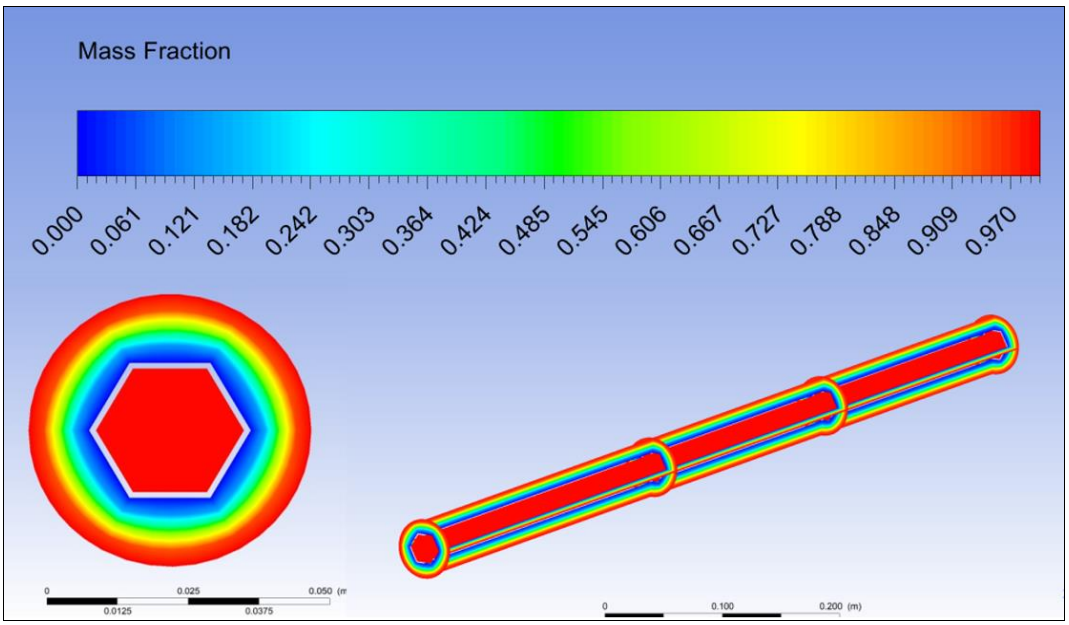

F. The mass fraction of the hexagonal tube

Fig 7: Mass fraction contour for six geometric shapes test.

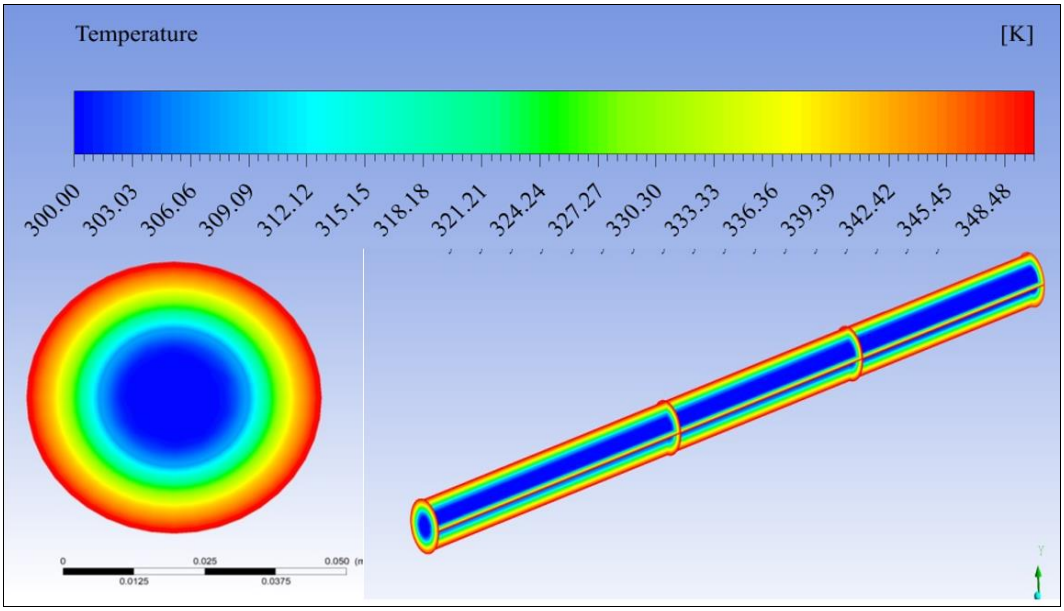

A. Temperature of the circular tube

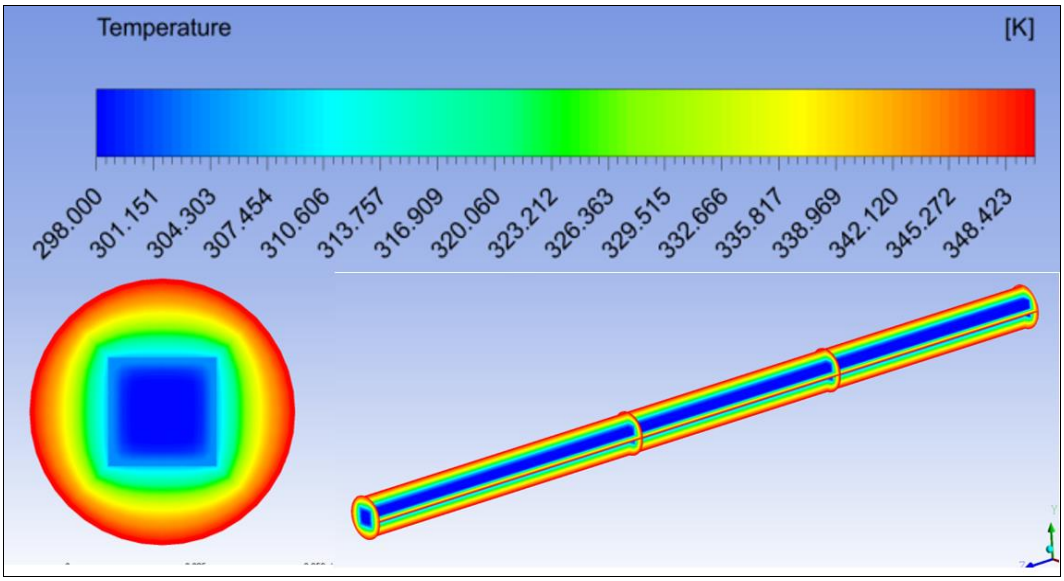

B. Temperature of the Square tube

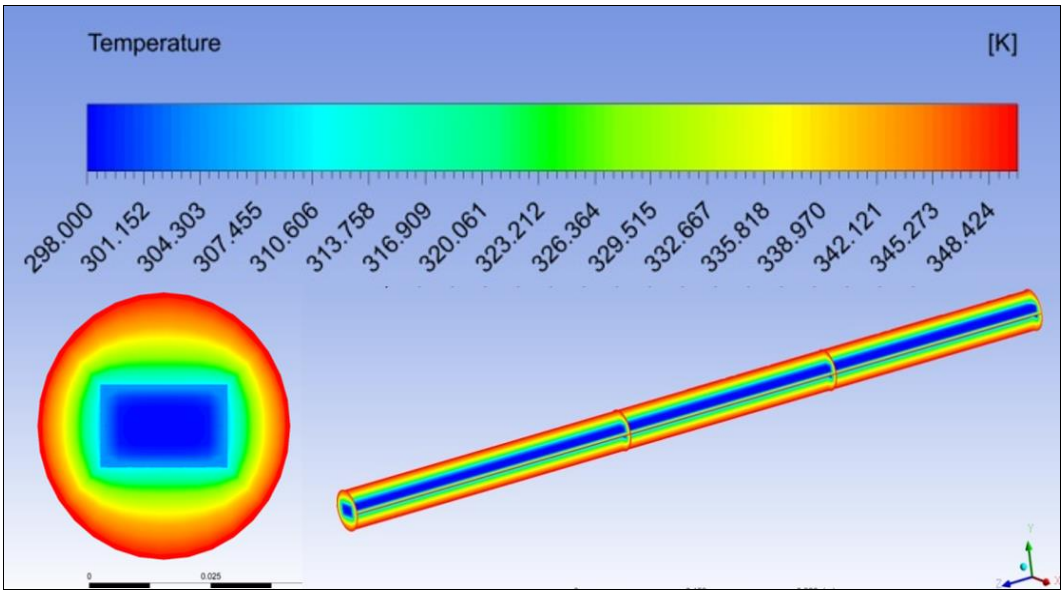

C. Temperature of the rectangular tube

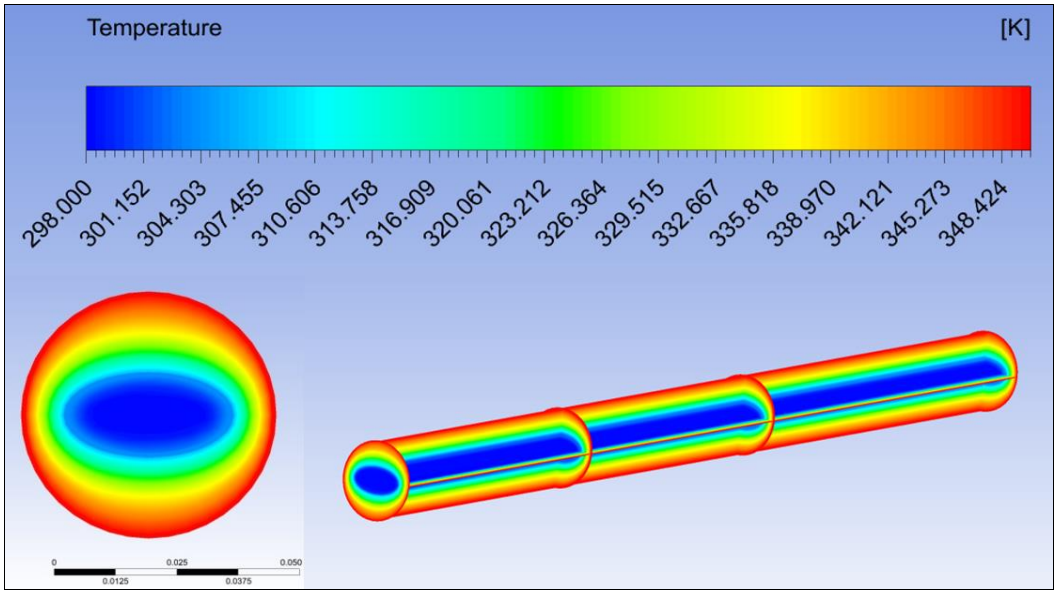

D. Temperature of the elliptical tube

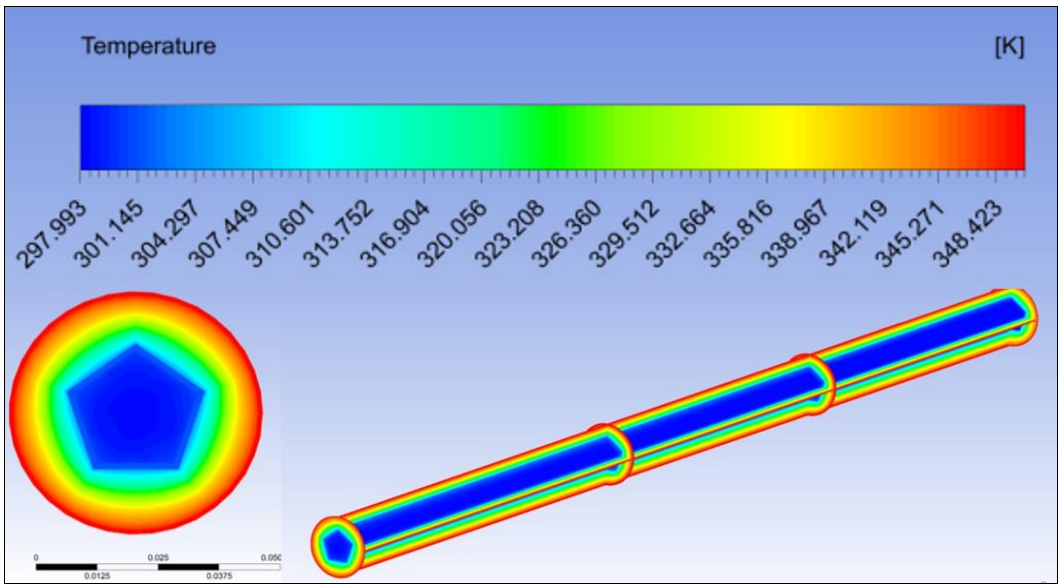

E. Temperature of the pentagonal tube

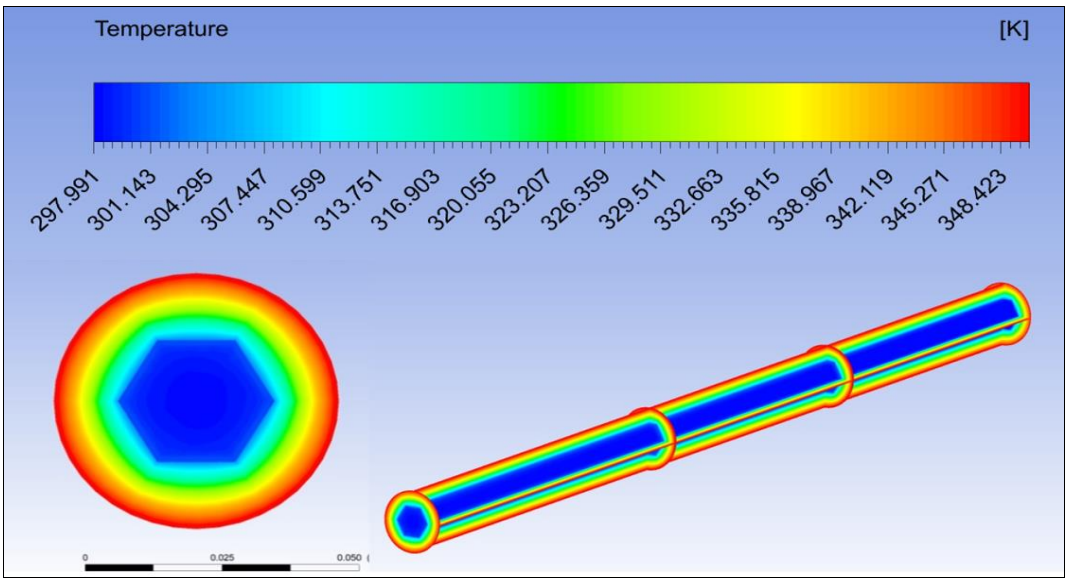

F. Temperature of the hexagonal tube

Fig 8: Theoretical temperature contour for six geometric shapes test.

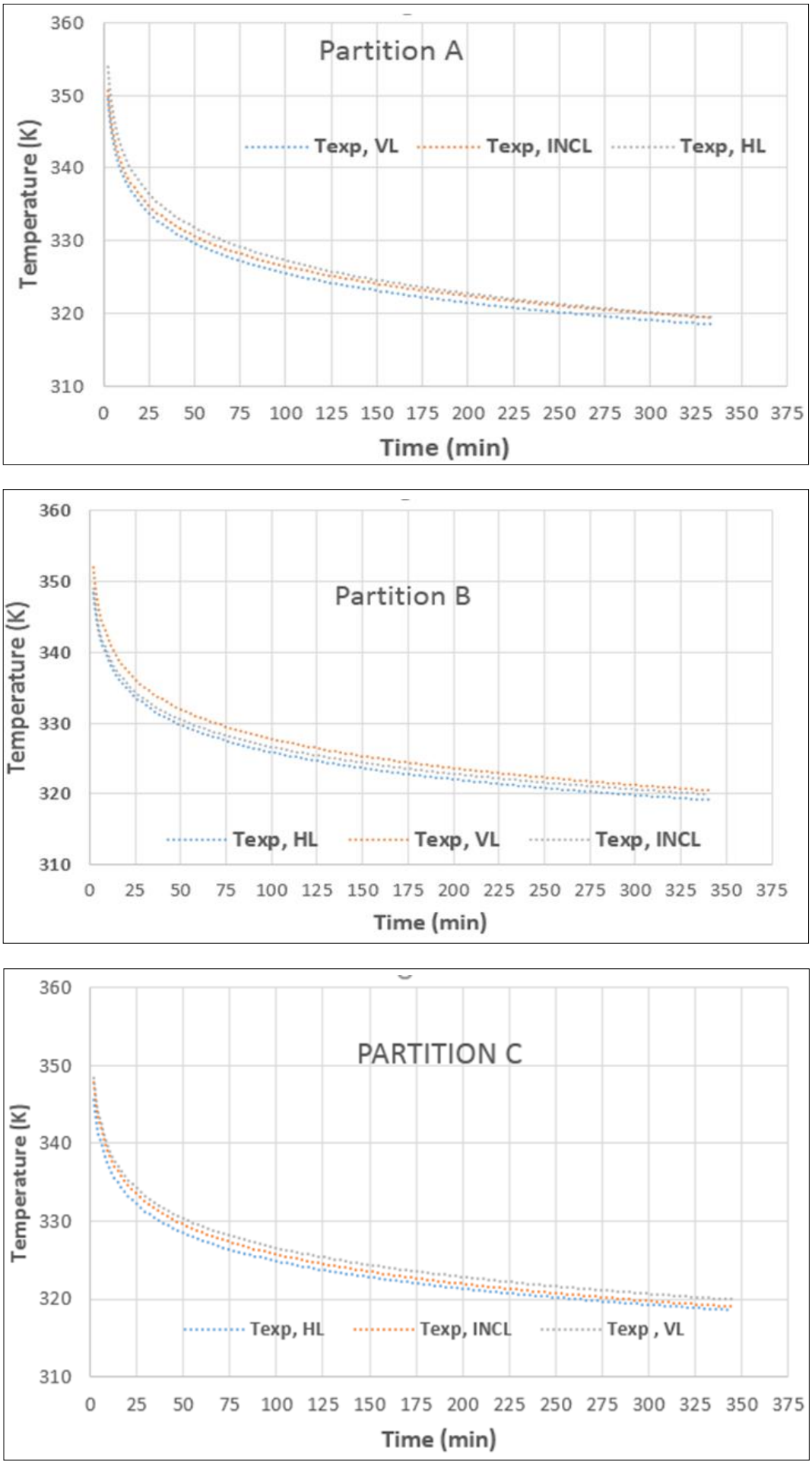

Fig 9: Temperature variation with time at three partitions of LHTES unit (A, B, and C) with circular inner tube for discharging process

4. Conclusions

This study investigates the thermal performance of the LHTES unit during the discharge process by analyzing different geometric configurations of the inner tube, including a circular tube, a square tube, a rectangular tube, an oval tube, a pentagonal tube, as well as a hexagonal tube. The analysis derives insights from both experimental data and numerical simulations. Several conclusions can be drawn: 1. Due to buoyant forces, natural convection prevails at the first heat transfer for all geometries investigated throughout the solidification process. Next, heat transfer changes to conduction, which takes longer for solidification to occur. The reaction delay in the discharge process time can be attributed to the larger distance between the circular wall and the center of the tube in this geometry compared to other configurations.

Label

Symbol	Notation	Unit
Amush	Mushy Zone Constant	-
C_p	Specific Heat Capacity	
pl	The liquid Phase	
ps	The Solid Phase	
F	Liquid Fraction Factor	-
g	The Gravitational Acceleration	m/s^2
h	Total Volumetric Enthalpy	kJ/ kg
h	The Sensible Enthalpy	kJ/ kg
href	The Enthalpy at the Reference Temperature	kJ/ kg
k	Thermal Conductivity of the PCM	W / m ^oC
L	The Latent Heat of the PCM	kJ/ kg
M	Mass	kg
h,e.	Heat Exchanger	
PCM	PCM	
$\dot{m}$	Mass Flow Rate	kg/s
P	Pressure	pa
q	Thermal Instantaneous Energy of Water	kJ/ sec
ch	Charging	c
dis	Discharging	
Q	Thermal Accumulative Energy of Water	kJ
ch	Melting	
dis	Discharging	
$Q_{max,\ ch}$	Max Theoretical Energy of PCM During Melting	kJ
$Q_{max,\ dis}$	Max Theoretical Energy of PCM During Solidification	kJ
$Q_{PCM,\ ch}$	Melting Thermal Accumulative Energy of PCM	kJ
$Q_{PCM,\ dis}$	Solidification Thermal Accumulative Energy of PCM	kJ
M	Global Source Term	J
T	Temperature	^oC
ini	*Initial of PCM*	
end	*End of PCM*	
w,in	*Inlet of Water*	
w,out	*Outlet of Water*	
T_0	*The Operating Temperature of the PCM*	*oC*
liquidus	*Liquid of the PCM*	
T_m	*Melting Temperature of the PCM*	^oC
ref	*Reference*	
solidus	*Solid of the PCM*	
t	*Time*	*s*
U	*HTF Velocity*	m/s

5. References

1. Du K, Calautit J, Wang Z, Wu Y, Liu H. A review of the applications of phase change materials in cooling, heating and power generation in different temperature ranges. Applied Energy. 2018;220:242-273.
2. Sayekar A, Mali A, Wadekar N, Nalawade P, Patil S. A Review on PCM heat exchanger using paraffin wax. Journal of Modern Thermodynamics in Mechanical System; c2019.
3. Alva G, Lin Y, Fang G. An overview of thermal energy storage systems. Energy. 2018;144:341-378.
4. Senthil, Ramalingam, Cheralathan M. Melting and solidification of paraffin wax in a concentric tube PCM Storage for Solar Thermal Collector. International Journal of Chemical. 2016;14(4):2634-2640.
5. Jesumathy SP, Udayakumar M, Suresh S, Jegadheeswaran S. An experimental study on heat transfer characteristics of paraffin wax in horizontal double pipe heat latent heat storage unit. Journal of the Taiwan Institute of Chemical Engineers. 2014;45(4):1298-1306.
6. Rathod MK, Banerjee J. Experimental investigations on latent heat storage unit using paraffin wax as phase change material. Experimental Heat Transfer. 2014;27(1):40-55.
7. Wang Y, Wang L, Xie N, Lin X, Chen H. Experimental study on the melting and solidification behavior of erythritol in a vertical shell-and-tube latent heat thermal storage unit. International Journal of Heat and Mass Transfer. 2016;99:770-781.

8. Jalil JM, Salih SM. Analysis of thermal and insulation performance of double glazed window doped with paraffin wax. Engineering and Technology Journal. 2020;38(3A):383-393.
9. Tangsiriratana E, Skolpap W, Patterson RJ, Sriprapha K. Thermal properties and behavior of micro-encapsulated sugarcane wax phase change material. Heliyon. 2019;5:8
10. Abed AH. Thermal storage efficiency enhancement for solar air heater using a combined SHSM and PCM Cylindrical capsules system: Experimental Investigation. Engineering and Technology Journal. 2016;34(5A):999-1011.
11. Abbas H, Jalil JM, Ahmed ST. Experimental investigation of the optimal location of PCM capsules in a hollow brick wall. Engineering and Technology Journal. 2021;39(5A):846-858.
12. Mahdi MS, Mahood HB, Hasan AF, Khadom AA, Campbell AN. Numerical study on the effect of the location of the phase change material in a concentric double pipe latent heat thermal energy storage unit. Thermal Science and Engineering Progress. 2019;11:40-49.
13. Sadeghi HM, Babayan M, Chamkha A. Investigation of using multi-layer PCMs in the tubular heat exchanger with periodic heat transfer boundary condition. International Journal of Heat and Mass Transfer. 2020;147:118970.
14. Liu Z, Sun X, Ma C. Experimental study of the characteristics of solidification of stearic acid in an annulus and its thermal conductivity enhancement. Energy Conversion and Management. 2005;46(6):971-984.
15. Alshara AK, Kadhim MK. Numerical investigation of energy storage in packed bed of cylindrical capsules of PCM. Engineering and Technology Journal. 2014;32(2):494-510.
16. Elmeriah A, Nehari D, Aichouni M. Thermo-convective study of a shell and tube thermal energy storage unit. Periodica Polytechnica Mechanical Engineering. 2018;62(2):101-109.
17. Avci M, Yazici MY. Experimental study of thermal energy storage characteristics of a paraffin in a horizontal tube-in-shell storage unit. Energy Conversion and Management. 2013;73:271-277.
18. Agarwal A, Sarviya RM. An experimental investigation of shell and tube latent heat storage for solar dryer using paraffin wax as heat storage material. Engineering Science and Technology, an International Journal. 2016;19(1):619-631.
19. Seddegh S, Joybari MM, Wang X, Haghighat F. Experimental and numerical characterization of natural convection in a vertical shell-and tube latent thermal energy storage system. Sustainable Cities and Society. 2017;35:13-24.
20. Hosseini MJ, Rahimi M, Bahrampoury R. Experimental and computational evolution of a shell and tube heat exchanger as a PCM Thermal Storage System. International Communications in Heat and Mass Transfer. 2014;50:128-136.
21. Yazici MY, Avci M, Aydin O, Akgun M. On the effect of eccentricity of a horizontal tube-in-shell storage unit on solidification of a PCM. Applied Thermal Engineering. 2014;64(1-2):1-9.
22. Esapour M, Hosseini MJ, Ranjbar AA, Pahamli Y, Bahrampoury R. Phase change in multi-tube heat exchangers. Renewable Energy. 2016;85:1017-1025.
23. Kousha N, Rahimi M, Pakrouh R, Bahrampoury R. Experimental investigation of phase change in a multitube heat exchanger. Journal of Energy Storage. 2019;23:292-304.
24. He Z, Wan Q, Wang Z, Zhang J, Yi S. The numerical simulation and experimental study of heat release in a heat storage system with various diameters of aluminum tubes. Heliyon. 2019;5:10.
25. Shen G, Wang X, Chan A. Experimental investigation of heat transfer characteristics in a vertical multi-tube latent heat thermal energy storage system. Energy Procedia. 2019;160:332-339.
26. Kibria MA, Anisur MR, Mahfuz MH, Saidur R, Metselaar IH. Numerical and experimental investigation of heat transfer in a shell and tube thermal energy storage system. International Communications in Heat and Mass Transfer. 2014;53:71-78.
27. Korawan AD, Soeparman S, Wijayanti W, Widhiyanuriyawan D. 3D numerical and experimental study on paraffin wax melting in thermal storage for the nozzle-and-shell, tube-and-shell, and reducer-and-shell models. Modelling and Simulation in Engineering; c2017.
28. Seddegh S, Wang X, Henderson AD. Numerical investigation of heat transfer mechanism in a vertical shell and tube latent heat energy storage system. Applied Thermal Engineering. 2015;87:698-706.
29. Kousha N, Hosseini MJ, Aligoodarz MR, Pakrouh R, Bahrampoury R. Effect of inclination angle on the performance of a shell and tube heat storage unit-An experimental study. Applied Thermal Engineering. 2017;112:1497-1509.
30. Mehta DS, Solanki K, Rathod MK, Banerjee J. Influence of orientation on thermal performance of shell and tube latent heat storage unit. Applied Thermal Engineering. 2019;157:113719.
31. Al Siyabi I, Khanna S, Mallick T, Sundaram S. An experimental and numerical study on the effect of inclination angle of phase change materials thermal energy storage system. Journal of Energy Storage. 2019;23:57-68.
32. Ajarostaghi M, Soheil S, Delavar MA, Dolati A. Numerical investigation of melting process in Phase Change Material (PCM) cylindrical storage considering different geometries. Heat Transf. Res. 2017;48:1515-1529.
33. Da Veiga WR, Meyer JP. Semicircular heat exchanger used in a water heated condenser pump.
34. Al-Jabair SJH, Al-Taee AAH. Experimental study of heat transfer coefficients of shell and helically coiled tube heat exchangers. Engineering and Technology Journal. 2013;31(1):172-196.
35. Longeon M, Soupart A, Fourmigué JF, Bruch A, Marty P. Experimental and numerical study of annular PCM Storage in the presence of natural convection. Applied Energy. 2013;112:175-184.
36. Hamza NF, Aljabair S. Evaluation of thermal performance factor by hybrid nanofluid and twisted tape inserts in heat exchanger. Heliyon. 2022;8:12.
37. Esapour M, hnezhad H, Darzi AAR, Jourabian M. Melting and solidification of PCM embedded in porous

metal foam in horizontal multi-tube heat storage system. Energy Conversion and Management. 2018;171:398-410.
38. Ghalambaz M, Zhang J. Conjugate solid-liquid phase change heat transfer in heatsink filled with phase change material-metal foam. International Journal of Heat and Mass Transfer. 2020;146:118832.
39. Albaldawi RA, Shyaa AK, Hammendy BM. Experimental study on the effect of insertion of copper lessing rings in Phase Change Material (PCM) on the performance of thermal energy storage unit. AlKhwarizmi Engineering Journal. 2015;11(4):60-72.
40. Jourabian M, Darzi AAR, Akbari O, Toghraie D. The enthalpy-based LATTICE BOLTZMANN METHOD (LBM) for simulation of NePCM melting in inclined elliptical annulus. Physica A: Statistical Mechanics and its Applications. 2020;548:123887.
41. Wang WW, Zhang K, Wang LB, He YL. Numerical study of the heat charging and discharging characteristics of a shell-and-tube phase change heat storage unit. Applied Thermal Engineering. 2013;58(1-2):542-553.
42. Begum L, Hasan M, Vatistas GH. Energy storage in a complex heat storage unit using commercial grade phase change materials: Effect of convective heat transfer boundary conditions. Applied Thermal Engineering. 2018;131:621-641.
43. Akgün M, Aydın O, Kaygusuz K. Experimental study on melting/solidification characteristics of a paraffin as PCM. Energy Conversion and Management. 2007;48(2):669-678.
44. Jian-you L. Numerical and experimental investigation for heat transfer in triplex concentric tube with phase change material for thermal energy storage. Solar Energy. 2008;82(11):977-985.
45. Hosseini MJ, Ranjbar AA, Sedighi K, Rahimi M. A combined experimental and computational study on the melting behavior of a medium temperature phase change storage material inside shell and tube heat exchanger. International Communications in Heat and Mass Transfer. 2012;39(9):1416-1424.
46. Hosseini MJ, Rahimi M, Bahrampoury R. Experimental and computational evolution of a shell and tube heat exchanger as a PCM thermal storage system. International Communications in Heat and Mass Transfer. 2014;50:128-136.
47. Holman JP. Experimental Methods for Engineers. 8th ed. United States: McGraw-Hill Series in Mechanical Engineering; c2011.
48. Seddegh S, Wang X, Henderson AD. A comparative study of thermal behaviour of a horizontal and vertical shell-and-tube energy storage using phase change materials. Applied Thermal Engineering. 2016;93:348-358. https://doi.org/10.1016/j.applthermaleng.2015.09.107.